IEEE Access
Multidisciplinary ⋮ Rapid Review ⋮ Open Access Journal

Received 24 June 2024, accepted 9 August 2024, date of publication 20 August 2024, date of current version 2 September 2024.

Digital Object Identifier 10.1109/ACCESS.2024.3446644

RESEARCH ARTICLE

A CPW-Based Novel SSPP Reflectionless Low-Pass Notch Filter With Loaded Interdigitated Coupling Structure

YUAN CAO, YUMING LU, SONGFENG YIN, (Student Member, IEEE), AND XIAO HU
School of Electrical and Control Engineering, Liaoning Technical University, Huludao 125100, China

Corresponding author: Yuming Lu (luyuming0405@163.com)

This work was supported by the National Natural Science Foundation of China under Grant 62173171.

ABSTRACT This study proposes a novel spoof surface plasmon polariton (SSPP) transmission line unit based on a coplanar waveguide (CPW) design. The dispersion relationship is derived from its equivalent circuit, and a low-pass notch filter is designed accordingly, operating in the frequency range of 0 GHz to 4.45 GHz, effectively blocking the transmission signal at 2.4 GHz. The filter has the advantages of a compact size, high transmission efficiency, and compact structure. The mode transition from quasi-transverse electromagnetic (TEM) waves in CPW to transverse magnetic (TM) waves in the SSPP waveguide is achieved using a centrally symmetric linear gradient groove structure. For the first time within the scope of this study, we propose a novel method for forming notch filters that involves radiating signals of selected frequencies into free space to create notch, thereby eliminating the negative effects of the reflected signals at notch point. This study achieves signal radiation at 2.4 GHz to free space, forming a notch, by loading an interdigitated coupling structure on the backside of the filter. The relationship between finger length and resonant frequency enables the reconfigurability of the filtering band. To validate the accuracy of the proposed filter, a prototype filter is fabricated and tested in this frequency range. The measurement results are consistent with the analytical results.

INDEX TERMS Spoof surface plasmon polariton, low-pass notch filter, reflectionless, radiation, interdigitated coupling structure.

I. INTRODUCTION

Surface plasmon polaritons (SPPs) are a type of surface wave propagating at the interface between a metal and a dielectric. The field strength of SPPs decays exponentially away from the interface, exhibiting strong confinement and local wave enhancement [1], [2]. Typically, the SPP modes can only be excited at the visible and near-infrared wavelengths. Owing to the perfect conductive properties of metals in the high-frequency range, these modes cannot exist at microwave or terahertz wavelengths [3], [4]. To extend the advantages and applications of SPPs from optical frequencies to the aforementioned lower frequencies, researchers have proposed the use of spoof surface plasmon polaritons (SSPPs) employing three-dimensional periodic metal or dielectric structures. The dispersion characteristics and wave propagation properties of this structure are similar to those of optical fields, particularly their ability to confine electromagnetic fields within sub-wavelength structures [5], [6], [7], [8]. In recent years, a series of two-dimensional planar periodic structures, such as sub-wavelength periodic groove lines, have increasingly replaced three-dimensional structures, exhibiting excellent propagation performance. Moreover, by appropriately configuring the structural parameters, the transmission bandwidth and characteristics of the SSPP structure can be better specified and satisfied, thereby providing convenient conditions for the design of passive microwave devices [9], [10], [11], [12].

As is well known, filters are the foundation and essential components of microwave and wireless communication systems. Traditional filters typically employ transmission

The associate editor coordinating the review of this manuscript and approving it for publication was Dušan Grujić.

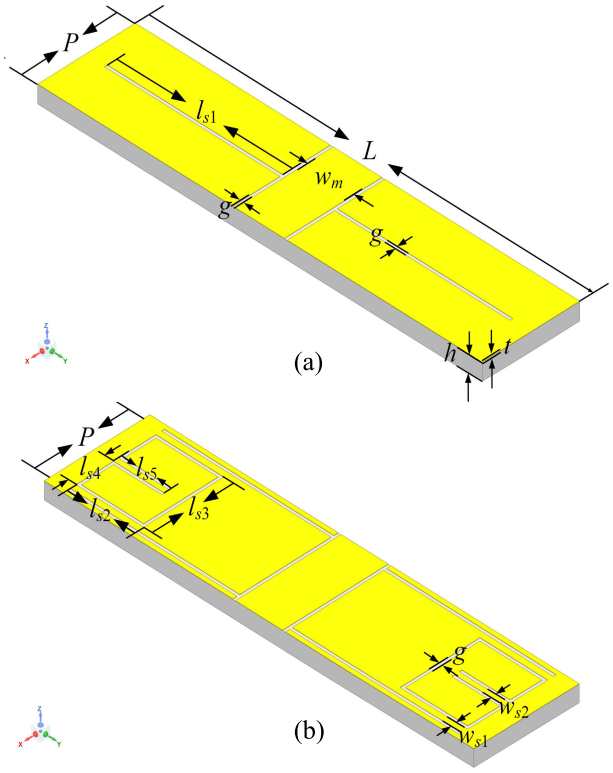

FIGURE 1. SSPP transmission line unit structure based on CPW (a) Conventional transmission line unit (b) Novel transmission line unit.

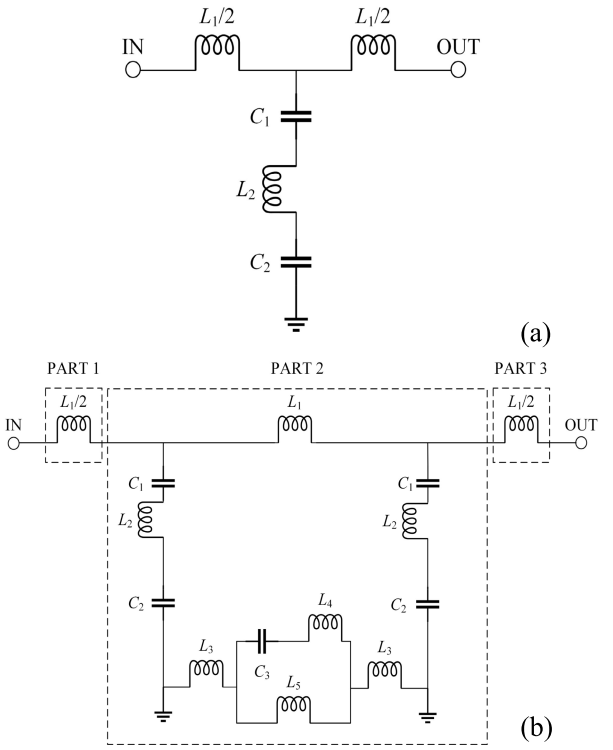

FIGURE 2. Equivalent circuits of SSPP transmission line unit (a) Conventional transmission line unit (b) Novel transmission line unit.

line structures such as microstrip lines (MSL) and coplanar waveguides (CPW). the application of microwave frequencies is becoming increasingly compact in today's increasingly advanced technologies for communication and satellite systems. To mitigate the impact of signal interference and adapt to the development of integrated circuits, research on miniaturized bandstop filters has become a popular focus [13], [14], [15]. In recent years, a series of SSPP notch filters have been designed. Reference [13] proposes a bandstop filter achieved by loading gaps between periodic units to form an equivalent capacitor. However, this structure becomes oversized owing to the inclusion of gaps. Reference [14] proposed a notch filter by embedding small H-shaped conductors inside a slot to form a complementary split-ring resonator (CSRR) in conjunction with waveguide conductors. However, this structure has a complex transition section, that leads to poor impedance matching in the low-frequency range. Reference [15] proposed loading a folded groove structure into traditional rectangular transmission line units, lowering the structure's cutoff frequency by increasing the current path, thus achieving device miniaturization to some extent.

In current filter designs, the common approach for introducing notches is to load resonators externally onto the transmission line, creating a total reflection states within a predefined frequency range. This results in reflected signals at the notch, which affect the performance of the filter. For example, signals at the notch point reflected back to the source end can cause signal loss, leading to a decline in overall system performance. The reflected signals at the notch interfering with the normal signals in the transmission direction created a three-dimensional ripple effect, which causes unevenness in the frequency response. Additionally, irregularities in the flatness of the notch or at the edges of the notch may occur owing to reflected signals. To address the above issues and improve the performance of the filter, this study proposes a new design approach for radiating signals at the notch point into free space instead of reflecting them back to the incident end. This innovative design overcomes the challenges associated with the degradation of the filter performance, as mentioned earlier. Based on the SSPP unit structure proposed in this study, a novel SSPP low-pass filter with a passband range of 0 GHz to 4.74 GHz is designed. It achieves downsizing by lowering the cutoff frequency without increasing structural size. By loading resonant structures on the backside of the filter, the 2.4 GHz signal is radiated into free space, thereby forming a notch. Compared with conventional notch filters, the filter in this study exhibited no reflected signal within the notch at the resonance point. This eliminates the negative impact of the reflected signal and provides a new design approach for notch filters. This approach has broad application prospects in future research on filters.

II. ANALYSIS OF A NOVEL SSPP TRANSMISSION LINE UNIT BASED ON CPW

The conventional SSPP transmission line unit based on CPW (Type A) is illustrated in Figure 1(a). It features a central

TABLE 1. Values of structural parameters of the SSPP transmission line unit (Units: mm).

Parameter	value	Parameter	value
g	0.15	w_m	2.5
w_{s1}	0.3	w_{s2}	0.25
l_{s1}	9	l_{s2}	2.25
l_{s3}	4.25	l_{s4}	2
l_{s5}	1.8	L	22.8
h	0.8	t	0.018
P	5		

CPW transmission line, and two symmetric linear groove structures are etched on the CPW GND. To maintain the characteristic impedance $Z_0 = 50\ \Omega$, the width of the central transmission line is denoted by wm, and the gap width between the central transmission line and GND is denoted by g. The dielectric substrate utilized in this study was ROGERS RO4350B, with a relative permittivity of $\varepsilon_r = 3.66$, and a loss tangent of $\tan\delta = 0.0037$. The thickness of the dielectric substrate is denoted by h, and a thin copper film is deposited on top of the dielectric substrate with a thickness of t. The symmetric groove structure had a length l_{s1} and width g. The transmission line unit has length P and width L. The cutoff frequency of this structure can be determined using l_{s1}.

The novel transmission line unit proposed in this study (Type B) incorporates a folded groove structure between the two linear groove structures based on the conventional structure. Its top aligns with the top of the symmetric groove structure; its top horizontal groove length is denoted by l_{s4}, and its vertical groove length is denoted by l_{s5}. The width of the folded groove structure is denoted by g, the gap between the folded groove structure and linear groove structure is denoted by w_{s1}, and the gap within the folded groove is denoted by w_{s2}. The overall structural dimensions of the novel SSPP transmission line unit were the same as those of the conventional line unit. All the specific numerical values of structural parameters are listed in Table 1.

The equivalent LC circuit of the novel SSPP transmission line unit is illustrated in Figure 2(b). This is the equivalent replacement of the CPW transmission line with a groove structure in the normal direction. Where L_1 represents the equivalent inductor of the CPW central transmission line, and the electromagnetic coupling between the central transmission line and ground plane is equivalent to a series structure of C_1 and L_2. C_2 represents the equivalent capacitor of the symmetric linear groove structure. L_3 is the equivalent inductor of linear and folded groove structures. The series-parallel circuit formed by C_3, L_4, and L_5 represents the equivalent circuit of the folded groove structure. The values of each component were obtained according to the optimization of the equivalent circuit in the ADS simulation software, as listed in Table 2.

Becauses the transmission line is composed of several cascaded transmission line units, the voltages and currents on both sides of the nth unit can be related using the A

TABLE 2. Values of each component of the equivalent circuit of the novel SSPP transmission line unit.

Parameter	value	Parameter	value
L_1	3.67nH	L_2	3.46nH
L_3	0.73nH	L_4	1.26nH
L_5	5.41nH	C_1	0.45pF
C_2	2.05pF	C_3	0.42pF

transmission matrix:

$$\begin{bmatrix} V_n \\ I_n \end{bmatrix} = \begin{bmatrix} A & B \\ C & D \end{bmatrix} \begin{bmatrix} V_{n+1} \\ -I_{n+1} \end{bmatrix} \tag{1}$$

$$\begin{bmatrix} A & B \\ C & D \end{bmatrix} = \begin{bmatrix} 1 & 0 \\ Y_{PART1} & 1 \end{bmatrix} \begin{bmatrix} A_{PART2} & B_{PART2} \\ C_{PART2} & D_{PART2} \end{bmatrix} \begin{bmatrix} 1 & 0 \\ Y_{PART3} & 1 \end{bmatrix} \tag{2}$$

Similarly, the A transmission matrix for the second part can be expressed in terms of the inductance of the equivalent circuit. The A transmission matrix for the second part is:

$$\begin{bmatrix} A_{PART2} & B_{PART2} \\ C_{PART2} & D_{PART2} \end{bmatrix} = \begin{bmatrix} 1 & 0 \\ Y_{PART2} & 1 \end{bmatrix} \tag{3}$$

Therefore, Y_{PART2} can be derived:

$$Y_{PART2} = \frac{j\Delta_1}{L_1\Delta_2 \left(\frac{\frac{j\omega C_1 C_2 (\omega^2 C_3 L_4 + \omega^2 C_3 L_5 - 1)}{\Delta_2}}{\Delta_1} - \frac{\Delta_1}{\omega C_1 C_2 L_1 (\omega^2 C_3 L_4 + \omega^2 C_3 L_5 - 1)} \right)} \tag{4}$$

In which, Δ_1 and Δ_2 are the defined operators:

$$\begin{aligned} \Delta_1 = {} & \omega^2 \begin{pmatrix} -C_1C_2L_2 - 2C_1C_2L_3 - C_1C_2L_5 \\ -2C_1C_3L_4 - 2C_1C_3L_5 - C_2C_3L_4 - C_2C_3L_5 \end{pmatrix} \\ & + \omega^4 C_1C_2C_3 \left(L_2L_4 + L_2L_5 + 2L_3L_4 + 2L_3L_5 + L_4L_5\right) \\ & + 2C_1 + C_2 \end{aligned} \tag{5}$$

$$\begin{aligned} \Delta_2 = {} & \omega^2 \begin{pmatrix} -2C_1C_2L_2 - 2C_1C_2L_3 - C_1C_2L_5 \\ -2C_1C_3L_4 - 2C_1C_3L_5 - 2C_2C_3L_4 - 2C_2C_3L_5 \end{pmatrix} \\ & + \omega^4 C_1C_2C_3 (2L_2L_4 + P2L_2L_5 + 2L_3L_4 + 2L_3L_5 + L_4L_5) \\ & + 2C_1 + 2C_2 \end{aligned} \tag{6}$$

Substituting Equation (4) into Equations (2) and (3), the A transmission matrix parameters of the transmission line unit can be obtained:

$$\begin{aligned} A &= 1 \\ B &= 0 \\ C &= \frac{4\Delta_1}{\omega C_1 C_2 L_1 \left(\omega^2 C_3 L_4 + \omega^2 C_3 L_5 - 1\right)} \\ &\quad + \frac{j\Delta_1}{\Delta_2 L_1 \left(\frac{\frac{j\omega C_1 C_2 (\omega^2 C_3 L_4 + \omega^2 C_3 L_5 - 1)}{\Delta_2}}{\Delta_1} - \frac{\Delta_1}{\omega C_1 C_2 L_1 (\omega^2 C_3 L_4 + \omega^2 C_3 L_5 - 1)} \right)} \\ D &= 1 \end{aligned} \tag{7}$$

At this point, the overall circuit can be equivalently represented as a transmission line, and the relationship is expressed

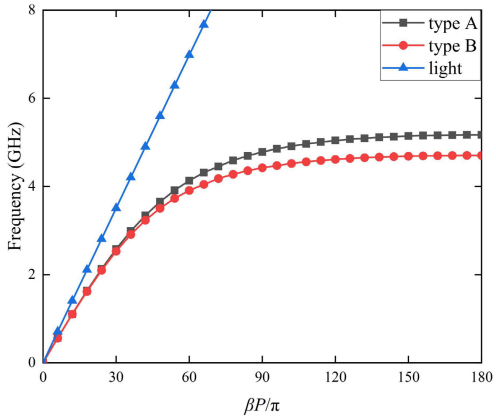

FIGURE 3. Dispersion curves of conventional SSPP transmission line unit (Type A) and novel SSPP transmission line unit (Type B).

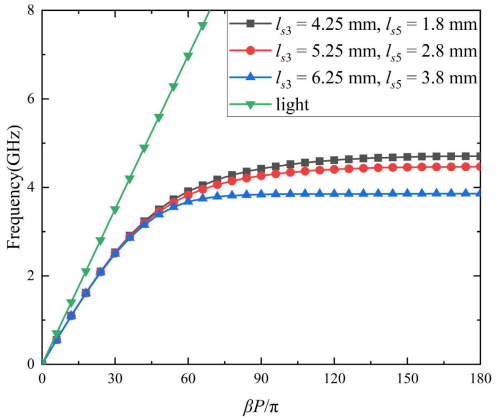

FIGURE 4. Dispersion curves of the novel SSPP transmission line unit with different l_{s3} and l_{s5}.

as follows:

$$C = \frac{j\sin(\beta P)}{Z_0} \tag{8}$$

where $Z_0 = 50\Omega$. Therefore, the dispersion relation for the novel SSPP transmission line unit is:

$$\beta = \frac{1}{P}\sin^{-1}(-jZ_0C) \tag{9}$$

The equivalent LC circuit of a conventional SSPP transmission line unit is shown in Figure 2(a). Following a similar analysis method, the A transmission matrix parameters for this structure can be obtained as follows:

$$\begin{bmatrix} V_n \\ I_n \end{bmatrix} = \begin{bmatrix} A_T & B_T \\ C_T & D_T \end{bmatrix} \begin{bmatrix} V_{n+1} \\ -I_{n+1} \end{bmatrix} \tag{10}$$

$$\begin{aligned} A_T &= 1 \\ B_T &= 0 \\ C_T &= j\omega C_1 + j\omega C_2 - 4j\omega L_1 - j\omega L_2 \\ D_T &= 1 \end{aligned} \tag{11}$$

At this point, the overall circuit can be equivalently represented as a transmission line, and the relationship is expressed as follows:

$$C_T = \frac{j\sin(\beta_1 P)}{Z_0} \tag{12}$$

Therefore, the dispersion relation for the conventional SSPP transmission line unit is:

$$\beta_1 = \frac{1}{P}\sin^{-1}(-jZ_0C_T) \tag{13}$$

By comparing Equations (9) and (13), it can be concluded that, without changing the overall size of the structure, the values that mainly affect the dispersion relation are C_3, L_4 and L_5. Essentially, the dispersion relation can be influenced by adjusting the structural parameters of the folding groove in the novel SSPP transmission line unit without increasing the overall size of the structure, thereby reducing the cutoff frequency and achieving structural miniaturization.

Simulations are conducted using the eigenmode solver in CST Microwave Studio to validate theoretical accuracy. The dispersion curves of both the conventional SSPP unit transmission line and novel unit transmission line are obtained, as illustrated in Figure 3. All the dispersion curves lie below the light line, signifying that the structure exhibits a significantly higher wave number in the propagation direction than in free space, which is consistent with slow-wave characteristics of the SSPP structure. The cutoff frequency of the conventional SSPP transmission line unit is 5.171 GHz, and the novel transmission line unit exhibits a notably lower cutoff frequency of 4.704 GHz. This validates the accuracy of the theoretical analysis.

In Equation (9), it can be observed that without changing the overall size of the structure, the parameters that mainly affect the dispersion relation are C_3, L_4 and L_5, and the influence of L_3 on the dispersion characteristics is relatively minor. This suggests that within the structural parameters of the folded groove w_{s1}, and l_{s3} are not the predominant parameters for modulating the dispersion characteristics. Furthermore, modifying w_{s2} to alter the value of L_4 leads to an enlargement of the overall lateral dimensions of the structure, which is not conducive to miniaturizing the structure. In summary, l_{s3} and l_{s5} are the key structural parameters that significantly affect the dispersion characteristics of this structure. Adjusting l_{s3} and l_{s5} from 4.25mm and 1.8mm to 6.25mm and 3.8mm, with a step size of 1mm for each adjustment, the resulting dispersion curves are shown in Figure 4. Increasing the dimensions of l_{s3} and l_{s5} is equivalent to altering the values of C_3, L_4 and L_5 in equivalent circuit. The reduction in the cutoff frequency of the transmission line unit further corroborates the accuracy of the theoretical analysis.

III. NOVEL FILTER ANALYSIS BASED ON THE NOVEL SSPP TRANSMISSION LINE UNIT

A. ANALYSIS OF LOW-PASS FILTER

The compact low-pass filter presented in Figure 5 is based on the previously proposed novel SSPP transmission line unit.

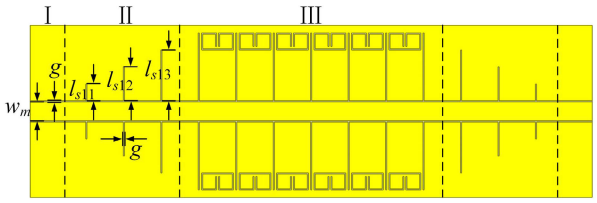

FIGURE 5. Schematic diagram of the SSPP low-pass filter structure.

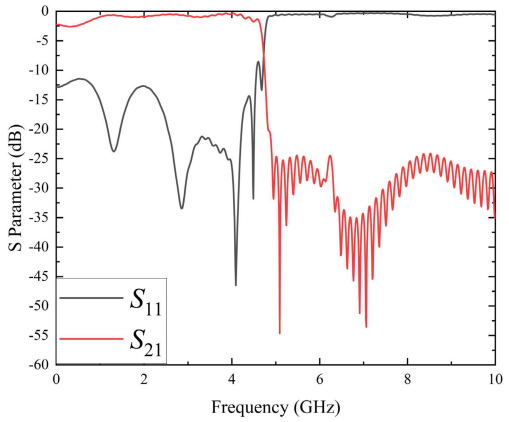

FIGURE 6. S_{11} and S_{21} simulations of the SSPP low-pass filter.

The overall length was $L_0 = 75$ mm and the overall width was $W_0 = 22.8$ mm.

The structure consists of three parts. The first part consists of a CPW structure. Considering compatibility with the 50 Ω impedance microwave system, in this part, the width of the center conductor strip is denoted as wm, and the gap between the center conductor strip and the ground plane is denoted as g, to achieve the characteristic impedance $Z_0 = 50\ \Omega$ at the port. The structural parameters are listed in Table 1. The length of this CPW part is $L_1 = 5$ mm.

The second part serves as a transition between CPW and SSPP transmission line. This part converts the quasi-transverse electromagnetic (TEM) wave of the CPW structure into the transverse magnetic (TM) wave of the SSPP structure. Owing to the slow-wave characteristics of SSPPs, there is a significant disparity in the wavenumbers between SSPP and CPW structure. However, as the gradient of the slot depth l_{s1k} in the straight grooves increased, the wavenumber in the transmission direction of the structure smoothly transitions. The symmetric straight groove structure lengths range from l_{s11} to l_{s13}. The specific values are as follows.

$$l_{s1k} = \frac{k}{4} l_{s1} \quad (k = 1, 2, 3) \tag{14}$$

The length of this transition part is $L_2 = 15$ mm.

The third part is an SSPP transmission line with a periodicity of 6. The length of the transmission line part is $L_3 = 35$ mm.

The simulation based on CST Microwave Studio is shown in Figure 6, which provides the return loss (S_{11}) and insertion loss (S_{21}) results for the proposed low-pass filter. Because the waveguide devices exhibit reciprocity, only the simulation results for S_{11} and S_{21} are presented. The simulation results reveal that within the frequency range of 0 GHz - 4.7 GHz, S_{11} consistently stays below −10 dB, exhibiting favorable reflection characteristic. Furthermore, within the frequency range of 0 GHz - 4.63 GHz, S_{21} is maintained predominantly below −2 dB, with a minimum value of −0.34 dB, exhibiting favorable transmission characteristic. As the frequency approaches the cutoff frequency, S_{21} rapidly decreases, indicating the excellent skirt characteristics of the filter. S_{21} is generally below −25 dB outside the passband. In summary, this filter demonstrates excellent transmission performance within the passband and effective out-of-band suppression outside the passband.

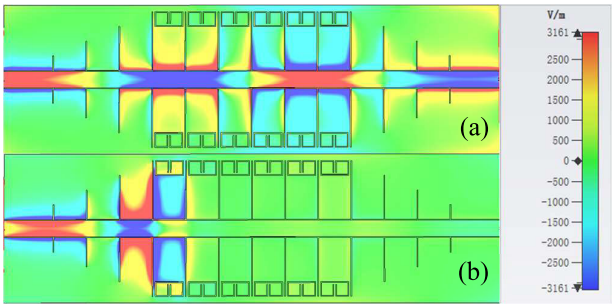

FIGURE 7. E_z of low-pass filter (a) 3GHz (b) 5GHz.

To gain a more intuitive understanding of the modal transmission characteristics and transmission performance of the SSPP low-pass filter, the z-direction electric field distribution $\boldsymbol{E_z}$ at $f_1 = 3$ GHz and $f_2 = 5$ GHz was simulated using a simulation software, as shown in Figure 7. f_1 and f_2 correspond to the in-band and out-of-band of the filter, respectively. In the passband, the waves propagated within the coplanar waveguide are effectively converted into SSPPs waves with shorter wavelengths, enabling efficient transmission. The electric field is tightly confined around the central transmission line and in the vicinity of the groove structure, exhibiting distinct TM mode characteristics. At $f_2 = 5$ GHz, although the guided waves can propagate within the coplanar waveguide, they cannot be transmitted through the SSPP transmission line because the frequency exceeds the cutoff frequency of the transmission line.

B. ANALYSIS OF LOW-PASS NOTCH FILTER LOADED WITH NOVEL INTERDIGITATED COUPLING STRUCTURE

To achieve the notch function for a specific frequency band in the passband, and address issues such as signal loss within the stopband and three-dimensional ripple effects to improve the filter performance, a low-pass notch filter structure based on the previous low-pass filter is proposed as shown in Figure 8, where the front-side of the notch filter is the same as that of the previously discussed low-pass filter as shown in Figure 8(a). Interdigitated coupling structures are loaded on the back side as shown in Figures 8(b) and 8(c). The

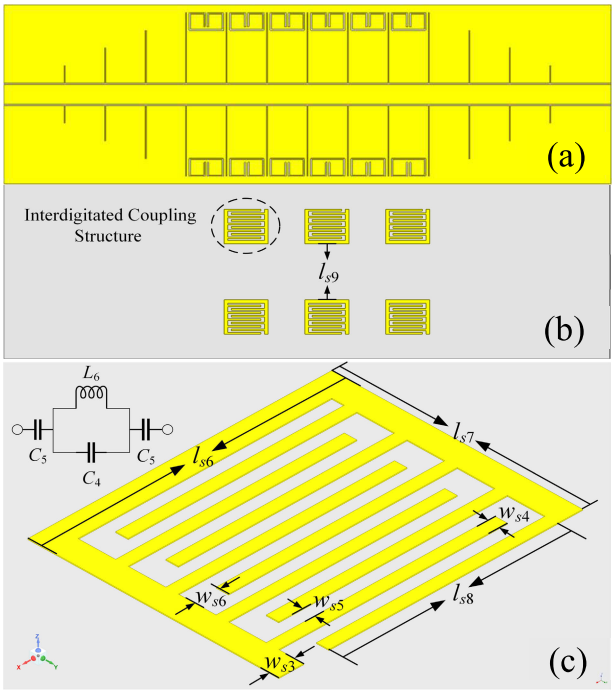

FIGURE 8. Structure of the novel low-pass notch filter with loaded interdigitated coupling (a) Front-side view (b) Back-side view (c) Enlarged view of the loaded interdigitated coupling structure.

TABLE 3. Values of interdigitated coupling structural parameters (Units: mm).

Parameter	value	Parameter	value
l_{s6}	5.45	l_{s7}	4.5
l_{s8}	4.1	l_{s9}	7.3
w_{s3}	0.45	w_{s4}	0.225
w_{s5}	0.225	w_{s6}	0.45

lateral length of the interdigitated coupling structure is l_{s6}, the longitudinal length is l_{s7}, the width of the connecting line is w_{s3}, the length of the coupling branch is l_{s8}, the width is w_{s4}, the coupling gap is w_{s5}, and the width between the interdigitated coupling and the connecting line is w_{s6}, the spacing in the normal direction to the transmission direction between the interdigital coupling structures is l_{s9}. The position of the interdigital coupling structures along the transmission direction correspond to the transmission line unit. The number of interdigitated coupling structures is $n = 6$. Specific values of the interdigitated coupling structural parameters are listed in Table 3.

The equivalent circuit of the interdigitated coupling structure is illustrated in Figure 8(c). In the equivalent circuit, the interdigitated coupling is equivalent to inductor L_6 in parallel with capacitor C_4. Additionally, considering that the interdigitated coupling structure is loaded on the back-side of the filter, capacitor C_5 is introduced to serve as an equivalent for the electric field between the interdigitated coupling structure and front-side structure.

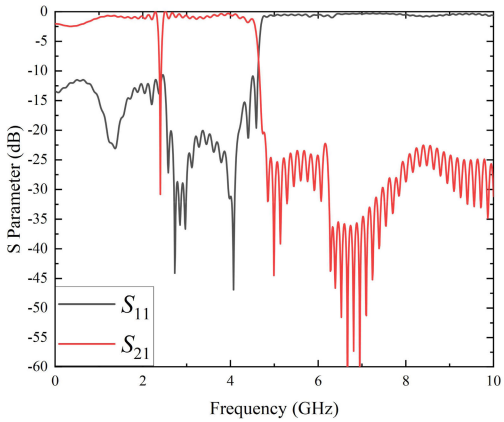

FIGURE 9. The simulation of S_{11} and S_{21} for the SSPP notch filter.

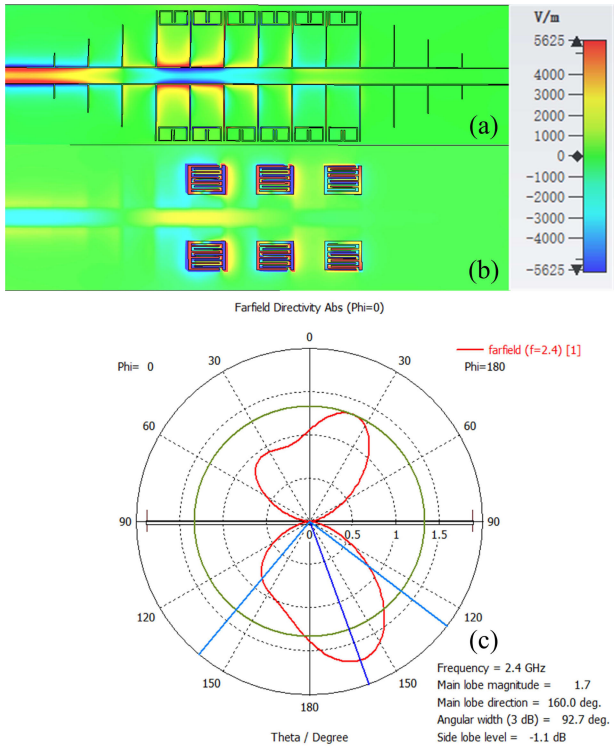

FIGURE 10. E_z of SSPP notch filter at $f_0 = 2.4$ GHz (a) Front-side (b) Back-side (c) Pattern of SSPP notch filter at $f_0 = 2.4$ GHz.

Without considering resistive losses, the resonant frequency of this structure is:

$$f_0 = \frac{1}{2\pi\sqrt{L_6 C_4}} \tag{15}$$

where, L_6 is determined by the length of the interdigitated coupling structure, and the value of C_4 is [16].

$$C_4 = \frac{\varepsilon_e 10^{-3} K(k)}{18\pi K'(k)} (N-1)\, l_{s8} \tag{16}$$

where N is the number of fingers of the interdigitated coupling structure and ε_e is the effective dielectric constant.

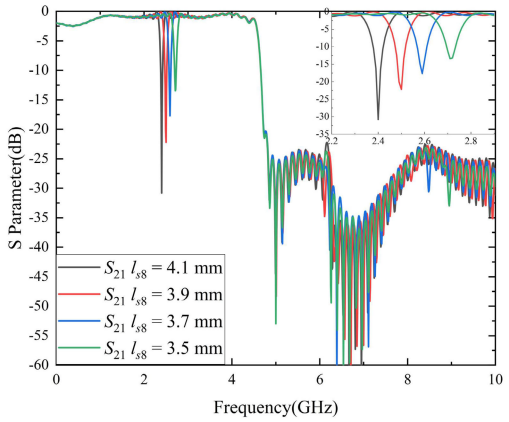

FIGURE 11. Simulation of S_{21} for SSPP notch filter with different values of l_{s8}.

$K(k)$ and $K'(k)$ are the complete elliptic functions of the first kind and their complementary functions, respectively, and modulus k is:

$$k = \tan^2\left[\frac{\pi w_{s4}}{4\,(w_{s4} - w_{s6})}\right] \tag{17}$$

A transmission zero is created at the resonant point in this structure to form the notch point.

The simulation results for S_{11} and S_{21} for this notch filter are shown in Figure 9. It can be clearly observed that the interdigitated coupling structure forms a notch at 2.4 GHz, where S_{21} is below −30 dB. However, at the frequency point, S_{11} is also below −10 dB, indicating that this resonator does not form a total reflection at the notch point, as in conventional structures. This is because the resonator attracts the transmitted signal at the resonance frequency.To a certain extent, the transmission line on the front side and the interdigital coupling structure on the back side can be equivalent to a set of CPW antennas. The interdigital coupling structure have the lowest equivalent impedance Z_{eq} at its resonant frequency, and the input signal is gathered at the interdigital coupling structure, which is equivalent to the coupling feeding of the antennas. Thus, the signal at the resonant frequency is radiated into free space, forming a reflectionless notch in this filter. Additionally, from Figure 9, it can be observed that at 2.4 GHz, the performance of the filter is not negatively affected by reflected signals, exhibiting regular notch edges and good skirt characteristics at this frequency.

The $\boldsymbol{E_z}$ and the radiation pattern of the structure, linearly scaled at 2.4 GHz, obtained through CST simulation are shown in Figure 10. It can be clearly observed from Figures 10(a) and 10(b) that at 2.4 GHz, the signal cannot propagate through the filter and instead is concentrated at the Interdigitated coupling structure on the back-side of the filter. In Figure 10(c) the deep blue line represents the elevation angle of the main lobe, and the light blue line represents the half-power point (3 dB point) of the main lobe. The main lobe of the radiation field at 2.4 GHz is located at the back-side of the filter, with a radiation gain of 1.7 dB and a 3 dB angular

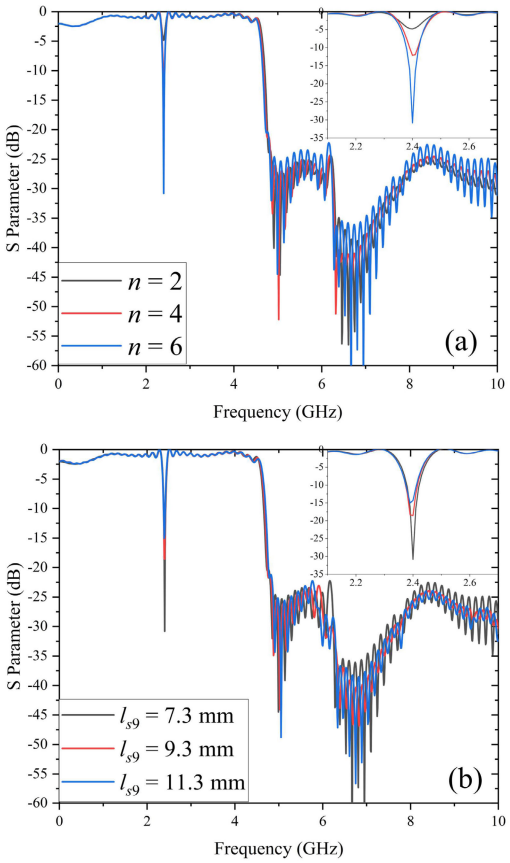

FIGURE 12. S_{21} of the low-pass notch filter under different interdigitated coupling structural parameters (a) n (b) l_{s9}.

width of 92.7 deg. The front side exhibits normal radiation loss only.

In addition, for this resonator structure, when the electrical length θ is constant, the resonant frequency f_0 exhibits the following relationship [17]:

$$\theta = l_{s8}\frac{f_0}{f} \tag{18}$$

$$\theta = l'_{s8}\frac{f'_0}{f} \tag{19}$$

Therefore, the relationship between the finger length l_{s8} and resonant frequency f_0 is as follows:

$$\frac{f_0}{l'_{s8}} = \frac{f'_0}{l_{s8}} \tag{20}$$

According to Equation (20), a linear relationship exists between l_{s8} and f_0. Therefore, by adjusting the value of l_{s8}, the position of the notch can be controlled.

Figure 11 shows the simulation of S_{21} for the SSPP notch filter at different values of l_{s8}. S_{11} consistently remains below −10 dB in the frequency range of 0 GHz - 4.7 GHz, and only the simulation of S_{21} is provided. By adjusting the value of l_{s8} from 4.1 mm to 3.5 mm, the notch frequency shifts from 2.4 GHz to 2.71 GHz, consistent with the results

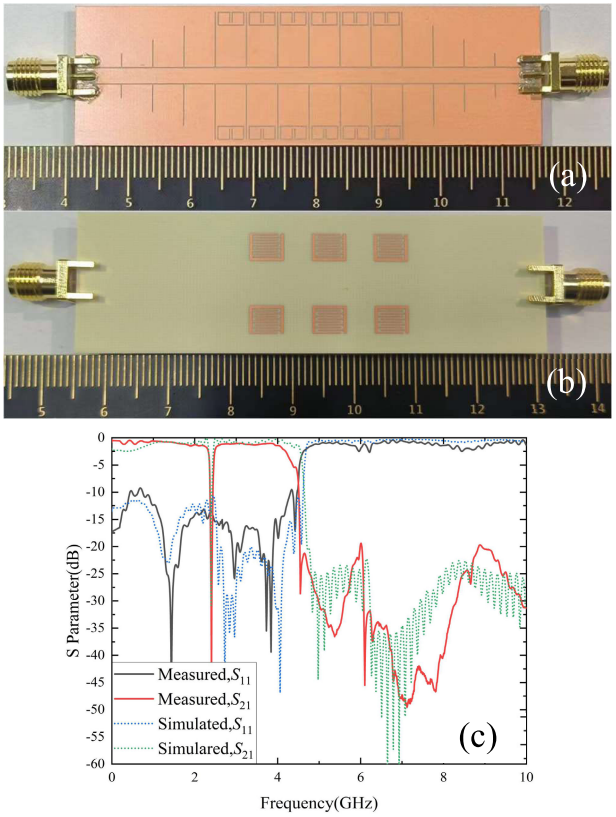

FIGURE 13. Physical schematic diagram of the low-pass notch filter (a) Front-side structure, (b) Back-side structure, (c) Measured and simulated S-parameters.

from Equation (20). In addition, reducing the value of l_{s8} shortens the length of the interdigitated coupling structure, thereby decreasing the coupling strength. Therefore, at the notch frequency, the value of S_{21} increases from −30.81 dB at 2.4 GHz to −13.46 dB at 2.71 GHz.

The simulated S_{21} results of the low-pass notch filter under different interdigitated coupling structures parameters are shown in Figure 12. From Figure 12(a), it can be observed that as n decreases from 6 to 2, the radiation capability of the structure diminishes, leading to a reduction in notch depth from −30 dB to −5 dB, which negatively affects the notch performance. From Figure 12(b), it can be observed that as l_{s9} increases from 7.3 mm to 11.3 mm, the radiation capability of the structure diminishes due to the interdigitated coupling structure moving farther from the central transmission line, which weakens its ability to absorb signals at the resonant frequency. Consequently, the notch depth decreases from −30 dB to −15 dB, which negatively affects the notch performance. In summary, the number and position of the interdigitated coupling structures have a significant negative impact on the notch performance at the resonant frequency.

Compared with conventional notch filters, the filter proposed in this study eliminates the reflection signals within the notch at the resonance point. This effectively eliminates disadvantages such as the three-dimensional ripple effect and signal loss caused by reflection signals, thereby providing a new design approach for notch filters.

TABLE 4. Comparison of this Article's filter with other SSPP notch filters (Λ_0 is the waveguide wavelength at the center frequency).

Ref.	Method	Frequency (GHz)	IL (dB)	RL (dB)	Roll-off rate (dB/GHz)	Size ($\lambda_0\times\lambda_0$)
[14]	Resonator total reflection	0-5.68 5.96-9.4	2 2.5	>10 >10	57.14	4.1×0.6
[15]	Resonator total reflection	0.7-1.1 2.05-2.48	2 1.5	>12 >15	49.16	0.76×0.21
[18]	Multi-Mods total reflection	4.35-6.2 6.7-8.12	1 1	>15 >15	91.37	1.14×0.52
[19]	Multi-Mods total reflection	5.8-8.71 8.95-11.01	1.5 1	>10 >10	141.37	1.35×0.68
This study	Resonator radiation	0-2.37 2.43-4.45	0.7 1.1	>15 >20	233.33	0.58×0.17

IV. RESULT

To verify the correctness of the theoretical and simulation results, a prototype of the low-pass notch filter was produced based on the above design, as shown in Figure 12. The front-side structure is shown in Figure 12(a), the back-side structure in Figure 12(b), and the results obtained using a vector analyzer in Figure 12(c). The measurement results exhibit good passband performance and out-of-band suppression. At the notch frequency, there are regular notching edges and excellent notching performance, which is consistent with the simulation results. This validates the theoretical and design outcomes of this study.

This study was compared with other SSPP notch filters, as listed in Table 4. Compared with other filters, this study features a lower insertion loss within the passband, indicating a flatter passband. In addition, this study is compared with other notch filters formed by loading resonant structures or exciting multiple modes. It is evident that our design exhibited an excellent roll-off rate in the stopband and smaller structural dimensions. In conclusion, through specific parameter comparisons, it is evident that this study exhibits superior performance compared with the current state of research.

V. CONCLUSION

In this study, we present a novel CPW-based SSPP low-pass notch filter. The dispersion relation of the transmission line unit is derived using the microwave network method based on the equivalent LC circuit of the transmission line unit. Based on the analysis of the transmission line unit, a low-pass filter with a working frequency range of 0 GHz to 4.45 GHz is proposed. This structure features compact size, structural efficiency, and high transmission efficiency. The electric field is mainly concentrated near the periodic unit, exhibiting the clear characteristics of the TM mode. Furthermore, to eliminate the negative impact of reflected signals at notch points in traditional notch filters on the filter performance,

it is proposed to radiate the signals at the notch points into free space instead of reflecting them back to the incident end. By loading the interdigitated coupling structure on the backside of the filter, the signal is radiated into free space at 2.4 GHz, forming a notch, which provides a new approach for notch filter design. Compared with conventional notch filters, the filter in this study exhibits no signal reflection at the notch points, thereby eliminating the negative effects caused by the reflected signals. This advancement holds promises for widespread application in future filter research.

REFERENCES

[1] T. W. Ebbesen, H. J. Lezec, H. F. Ghaemi, T. Thio, and P. A. Wolff, "Extraordinary optical transmission through sub-wavelength hole arrays," *Nature*, vol. 391, no. 6668, pp. 667–669, Feb. 1998.

[2] L. Yin, V. K. Vlasko-Vlasov, J. Pearson, J. M. Hiller, J. Hua, U. Welp, D. E. Brown, and C. W. Kimball, "Subwavelength focusing and guiding of surface plasmons," *Nano Lett.*, vol. 5, no. 7, pp. 1399–1402, Jun. 2005.

[3] N. Yu, Q. J. Wang, M. A. Kats, J. A. Fan, S. P. Khanna, L. Li, A. G. Davies, E. H. Linfield, and F. Capasso, "Designer spoof surface plasmon structures collimate terahertz laser beams," *Nature Mater.*, vol. 9, no. 9, pp. 730–735, Aug. 2010.

[4] M. E. Stewart, C. R. Anderton, L. B. Thompson, J. Maria, S. K. Gray, J. A. Rogers, and R. G. Nuzzo, "Nanostructured plasmonic sensors," *Chem. Rev.*, vol. 108, no. 2, pp. 494–521, Feb. 2008.

[5] F. J. Garcia-Vidal, L. Martín-Moreno, and J. B. Pendry, "Surfaces with holes in them: New plasmonic metamaterials," *J. Opt. A, Pure Appl. Opt.*, vol. 7, no. 2, pp. S97–S101, Jan. 2005.

[6] W. L. Barnes, A. Dereux, and T. W. Ebbesen, "Surface plasmon subwavelength optics," *Nature*, vol. 424, no. 6950, pp. 824–830, 2003.

[7] T. W. Ebbesen, C. Genet, and S. I. Bozhevolnyi, "Surface-plasmon circuitry," *Phys. Today*, vol. 61, no. 5, pp. 44–50, May 2008.

[8] X. Shen, T. J. Cui, D. Martin-Cano, and F. J. Garcia-Vidal, "Conformal surface plasmons propagating on ultrathin and flexible films," *Proc. Nat. Acad. Sci. USA*, vol. 110, no. 1, pp. 40–45, Jan. 2013.

[9] L. Liu, Z. Li, C. Gu, P. Ning, B. Xu, Z. Niu, and Y. Zhao, "Multi-channel composite spoof surface plasmon polaritons propagating along periodically corrugated metallic thin films," *J. Appl. Phys.*, vol. 116, no. 1, Jul. 2014, Art. no. 13501.

[10] C. R. Williams, S. R. Andrews, S. A. Maier, A. I. Fernández-Domínguez, L. Martín-Moreno, and F. J. García-Vidal, "Highly confined guiding of terahertz surface plasmon polaritons on structured metal surfaces," *Nature Photon.*, vol. 2, no. 3, pp. 175–179, Feb. 2008.

[11] M. Navarro-Cía, M. Beruete, S. Agrafiotis, F. Falcone, M. Sorolla, and S. A. Maier, "Broadband spoof plasmons and subwavelength electromagnetic energy confinement on ultrathin metafilms," *Opt. Exp.*, vol. 17, no. 20, p. 18184, Sep. 2009.

[12] T. Jiang, L. Shen, J.-J. Wu, T.-J. Yang, Z. Ruan, and L. Ran, "Realization of tightly confined channel plasmon polaritons at low frequencies," *Appl. Phys. Lett.*, vol. 99, no. 26, Dec. 2011.

[13] J. Y. Yin, J. Ren, H. C. Zhang, Q. Zhang, and T. J. Cui, "Capacitive-coupled series spoof surface plasmon polaritons," *Sci. Rep.*, vol. 6, no. 1, p. 24605, Apr. 2016.

[14] W. Li, Z. Qin, Y. Wang, L. Ye, and Y. Liu, "Spoof surface plasmonic waveguide and its band-rejection filter based on H-shaped slot units," *J. Phys. D, Appl. Phys.*, vol. 52, no. 36, Jul. 2019, Art. no. 365303.

[15] X. Zhang, S. Sun, Q. Yu, L. Wang, K. Liao, and S. Liu, "Novel high-efficiency and ultra-compact low-pass filter using double-layered spoof surface plasmon polaritons," *Microw. Opt. Technol. Lett.*, vol. 64, no. 6, pp. 1056–1061, Mar. 2022.

[16] Y. Peng and W. Zhang, "Compact sub-wavelength microstrip band-reject filter based on inter-digital capacitance loaded loop resonators," *Microw. Opt. Technol. Lett.*, vol. 52, no. 1, pp. 166–169, Jan. 2010.

[17] B. W. Xu, Q. Z. Quan, S. Y. Zheng, Y. X. Li, and W. Hong, "A coupler with simultaneously tunable phase, frequency and coupling coefficient," *IEEE Trans. Circuits Syst. II, Exp. Briefs*, vol. 69, no. 12, pp. 4759–4763, Dec. 2022, doi: 10.1109/TCSII.2022.3198637.

[18] S. Sun, Y. Cheng, H. Luo, F. Chen, and X. Li, "Notched-wideband bandpass filter based on spoof surface plasmon polaritons loaded with resonator structure," *Plasmonics*, vol. 18, no. 1, pp. 165–174, Feb. 2023.

[19] K.-D. Xu, S. Lu, Y.-J. Guo, and Q. Chen, "High-order mode of spoof surface plasmon polaritons and its application in bandpass filters," *IEEE Trans. Plasma Sci.*, vol. 49, no. 1, pp. 269–275, Jan. 2021, doi: 10.1109/TPS.2020.3043889.

YUAN CAO was born in Jilin, China, in 1982. She received the bachelor's, master's, and Ph.D. degrees in engineering from Dalian Maritime University, in 2005, 2008, and 2019, respectively. In 2011, she assumed the role of a Researcher in research of electromagnetic fields and microwave technology with Liaoning Technical University. In 2021, she was appointed as an Associate Professor with the School of Electrical and Control Engineering, Liaoning Technical University. She has contributed to academia with the publication of four SCI papers and three EI papers.

YUMING LU was born in Liaoning, China, in 2000. He received the bachelor's degree from Liaoning Technical University, in 2022, where he is currently pursuing the master's degree. His research interest includes design of RF devices based on spoof surface plasmons.

SONGFENG YIN (Student Member, IEEE) was born in Henan, China, in 1997. He received the bachelor's degree from Shangqiu Institute of Technology, in 2021. He is currently pursuing the master's degree with Liaoning Technical University. His research interest includes RF circuit design.

XIAO HU was born in Hubei, China. He received the bachelor's degree from Liaoning Technical University, China, in 2022, where he is currently pursuing the master's degree. His research interest includes microwave devices.